Target-oriented least-squares migration/inversion with sparseness constraints

Yaxun Tang

ABSTRACT

I pose the seismic imaging problem as an inverse problem and present a regularized inversion scheme that tries to overcome three main practical issues with the standard least-squares migration/inversion (LSI) approach, i.e., the high computational cost, the operator mismatch, and the poorly constrained solution due to a limited surface acquisition geometry. I show that the computational cost is considerably reduced by formulating the LSI problem in a target-oriented fashion and computing a truncated Hessian operator using the phase-encoding method. The second and third issues are mitigated by introducing a non-quadratic regularization operator that imposes sparseness to the model parameters. Numerical examples on the Marmousi model show that the sparseness constraint has the potential to effectively reduce the null space and produce an image with high resolution, but it also has the risk of over-penalizing weak reflections.

INTRODUCTION

Migration is an important and robust tool for imaging subsurface structures using reflection seismic data. However, migration operator is only the adjoint of the forward Born modeling operator (Lailly, 1983), which produces reliable structural information of the subsurface (assuming an accurate background velocity is known), but blurs the image because of the non-unitary nature of the Born modeling operator. To deblur the migrated image and correct the effects of limited acquisition geometry, complex overburden and bandlimited wavefields, the imaging problem can be treated as an inverse problem, which, instead of using the adjoint operator, uses the pseudo-inverse of the Born modeling operator to optimally reconstruct the reflectivity. This inversion-based imaging mehtod is also widely known as least-squares migration (Nemeth et al., 1999; Kuhl and Sacchi, 2003; Clapp, 2005; Valenciano, 2008).

The standard least-squares migration/inversion (LSI) approach tries to minimize an objective function defined in the data space, which compares the mismatch between the modeled and the observed primaries (Nemeth et al., 1999; Kuhl and Sacchi, 2003; Clapp, 2005). The objective function is then minimized with a gradient-based optimization solver, which iterates until an acceptable image is obtained. However, the data-space inversion scheme lacks flexibility and cannot be implemented in a target-oriented fashion. Full-domain migration/demigration has to be carried out within

each iteration; and the optimization converges slowly without a proper preconditioner. Therefore, the data-space inversion scheme is computationally challenging for large-scale applications.

One way to reduce the computational cost is by solving the LSI problem in a target-oriented fashion (Yu et al., 2006; Valenciano, 2008). This can be achieved by minimizing an objective function defined in the model space, instead of the data space. The target-oriented model-space formulation allows us to invert only areas of particular interest, such as subsalt regions, where potential reservoirs are located and migration often fails to provide reliable images. Solving the LSI in the model space requires explicitly computing the Hessian, the normal operator of the forward Born modeling operator. The full Hessian, however, is expensive to compute without certain approximations. Fortunately, as demonstrated by Valenciano (2008) and Tang and Biondi (2009), for a typical conventional acquisition geometry (shot records do not interfer), the Hessian matrix is sparse and diagonally dominant for most areas. Thus a truncated Hessian with a limited number of off-diagonal elements (the number is usually very small) can be used to approximate the exact Hessian for inverse filtering.

The truncated Hessian can be computed by storing the Green's functions (Valenciano, 2008), which, however, may bring considerable computational issues (e.g. disk storage, I/O and etc.), because the Green's functions can be huge for practical applications, especially in 3-D. To reduce the computational overburden, this paper computes the Hessian using the phase-encoding method (Tang, 2008b). As demonstrated by Tang (2008b) and Tang (2008a), computing the phase-encoded Hessian does not require storing any Green's functions and it is also more efficient: the cost for computing the receiver-side randomly phase-encoded Hessian is about one shot-profile migration, and if a mixed simultaneous phase-encoding strategy is used, the cost is about one plane-wave source migration.

Besides the computational cost, two main issues, i.e., the operator mismatch and the underdetermined nature of the seismic inverse problem, make the practical application of LSI less effective. The first issue often arises when our modeling operator is not sufficient to predict the physics of the data, for example, anisotropy or elasticity presents in the data but is not accurately modeled by our numerical operators. This can cause data-inconsistency problems. The second issue is due to the limited surface seismic acquisition geometry, which makes the inversion have an infinite number of solutions that fit the observed data equally well. Regularization is therefore important to stabilize the inversion and make it converge to geologically reasonable solutions. In this paper, I exploit the application of a non-quadratic regularization operator that imposes sparsness to the model space (Sacchi and Ulrych, 1995; Ulrych et al., 2001). The model-space sparsity is achieved by minimizing the model residual in the ℓ_1 or Cauchy norm, whose distribution is longer-tailed than the Gaussian distribution (the ℓ_2 norm), hence it penalizes weak energy and leads to spiky solutions (Amundsen, 1991). The application of the sparseness constraint to seismic imaging has also been reported by Tang (2006) and Wang and Sacchi (2007), who use it to regularize prestack image gathers. In this paper, however, I use it to regularize the prestack

image (zero subsurface offset) to enhance the resolution of the inverted reflectivity. I compare the one-way wave-equation inversion results on the Marmousi model regularized using the sparseness constraint with those regularized using a standard ℓ_2 norm damping. The experiments have been carried out on data sets synthesized using both one-way wave-equation Born modeling and two-way acoustic wave-equation finite-difference modeling. The first case represent the ideal scenario, where our modeling operator (one-way wave-equation propagator for this case) matches all the physics in the data. I show that both inversion schemes work well under this situation, and sparseness constrained inversion can offer slightly higher resolution. The second case is much more challenging for both schemes, because our modeling operator can not model all the complexities present in the data (e.g., amplitudes, multiples and etc.). My experiments show that under this difficult situation, the sparseness-constrained approach provides us a better inversion result for the Marmousi model, which suggests the importance of accurate model covariance (or the *a priori* information) for the LSI problem.

This paper is organized as follows: I first briefly review the theory of target-oriented LSI and phase-encoded Hessian, then I discuss the sparseness constraint which minimizes the model residual in the Cauchy norm. Finally I apply the regularized inversion scheme to the Marmousi model.

TARGET-ORIENTED LEAST-SQUARES MIGRATION

Within limits of the Born approximation of the acoustic wave equation, the seismic data can be modeled with a linear operator as follows

$$\mathbf{d} = \mathbf{L}\mathbf{m}, \tag{1}$$

where $\mathbf{d}$ is the modeled data, $\mathbf{L}$ is the Born modeling operator and $\mathbf{m}$ denotes the reflectivity of the subsurface (a perturbed quantity from the background velocity). The simplest way is to use the adjoint of the Born modeling operator to image the reflectivity $\mathbf{m}$ as follows:

$$\mathbf{m}_{\text{mig}} = \mathbf{L}'\mathbf{d}_{\text{obs}}, \tag{2}$$

where the superscript denotes the conjugate transpose and the subscript $_{\text{obs}}$ denotes observed data. However, migration produces unreliable images in areas of poor illumination. To get an optimally reconstructed image, we can invert equation 1 in the least-squares sense. The least-squares soltuion of equation 1 can be formally written as follows

$$\mathbf{m} = \mathbf{H}^{-1}\mathbf{m}_{\text{mig}}, \tag{3}$$

where $\mathbf{H} = \mathbf{L}'\mathbf{L}$ is the Hessian operator. Equation 3 has only symbolic meaning, because the Hessian is often singular and its inverse is not easy to obtain directly. A

more practical method is to reconstruct the reflectivity $\mathbf{m}$ through iterative inverse filtering by minimizing a model-space objective function defined as follows:

$$J(\mathbf{m}) = ||\mathbf{Hm} - \mathbf{m}_{\text{mig}}||_2^2, \tag{4}$$

where $||\cdot||_2$ denotes the ℓ_2 norm. Each component of the Hessian matrix $\mathbf{H}$ can be computed with the following equation, which is obtained by evaluating the operator $\mathbf{L'L}$ (Plessix and Mulder, 2004; Valenciano, 2008):

$$\begin{aligned} H(\mathbf{x},\mathbf{y}) = & \sum_{\omega} \omega^4 \sum_{\mathbf{x}_s} |f_s(\omega)|^2 G(\mathbf{x},\mathbf{x}_s,\omega) G'(\mathbf{y},\mathbf{x}_s,\omega) \\ \times & \sum_{\mathbf{x}_r} w(\mathbf{x}_r,\mathbf{x}_s) G(\mathbf{x},\mathbf{x}_r,\omega) G'(\mathbf{y},\mathbf{x}_r,\omega), \end{aligned} \tag{5}$$

where ω is the angular frequency, and $f_s(\omega)$ is the source function; $G(\mathbf{x},\mathbf{x}_s,\omega)$ and $G(\mathbf{x},\mathbf{x}_r,\omega)$ denote Green's functions connecting the source location $\mathbf{x}_s = (x_s, y_s, 0)$ and receiver location $\mathbf{x}_r = (x_r, y_r, 0)$ to the image point $\mathbf{x}$, respectively. We have similar definitions for $G(\mathbf{y},\mathbf{x}_s,\omega)$ and $G(\mathbf{y},\mathbf{x}_r,\omega)$, except that they define the Green's functions connecting the source and receiver locations to another image point $\mathbf{y}$ in the subsurface. Throughout this paper, we assume the Green's functions are computed by means of one-way wavefield extrapolation (Claerbout, 1985; Stoffa et al., 1990; Ristow and Rühl, 1994). But Green's functions obatined with other methods, such as the ray-based approach, the two-way wave-equation-based approah and etc., can also be used under this framework. The weighting factor $w(\mathbf{x}_s,\mathbf{x}_r)$ denotes the acquisition mask matrix (Tang, 2008a) defined as follows:

$$w(\mathbf{x}_r,\mathbf{x}_s) = \begin{cases} 1 & \text{if } \mathbf{x}_r \text{ is within the recording} \\ & \text{range of a shot at } \mathbf{x}_s; \\ 0 & \text{otherwise .} \end{cases} \tag{6}$$

When $\mathbf{x} = \mathbf{y}$, we obtain the diagonal elements of the Hessian; when $\mathbf{x} \neq \mathbf{y}$, we obtain the off-diagonal elements. A target-oriented truncated Hessian is obtained by computing the Hessian for $\mathbf{x}$'s that are within the target zone and a small number of $\mathbf{y}$'s that are close to each $\mathbf{x}$ (Valenciano, 2008).

HESSIAN BY PHASE ENCODING

The truncated Hessian operator can be computed by using equation 5, but direct implementation of equation 5 requires storing a huge number of Green's functions (especially in 3-D), which may bring computational challenges for large-scale applications. An alternative and also more efficient way is to compute the Hessian using the so-called phase-encoding method (Tang, 2008b,a), where equation 5 is structured into a similar form as that of the wave-equation migration, except for a modified boundary condition for the receiver wavefield and a modified imaging condition which correlates four wavefields instead of two. Doing so makes storing Green's functions unnecessary,

and the cost for computing a target-orineted wave-equation Hessian becomes comparable to one migration.

As further discussed by Tang (2008a), the phase-encoded Hessian is equivalent to the imaging Hessian in the generalized source and receiver domain, a transformed domian that is obtained by linear combination of the encoded sources and receivers. Different phase-encoded Hessian therefore can be obtained through different encoding strategies: if the encoding is performed in the source domain, we get the source-side encoded Hessian; if the encoding is performed in the receiver domain, we get the receiver-side encoded Hessian; if the encoding is performed in both source and receiver domain, we get the source- and receiver-side simultaneously encoded Hessian. One shortcoming of the encoding method, however, is that it also introduces undesired crosstalk artifacts, which may affect the convergence of the model-space based inversion (Tang, 2008b). The crosstalk artifacts can be effectively suppressed by carefully choosing the phase-encoding functions. As demonstrated by Tang (2008b,a), plane-wave-phase encoding or random-phase encoding or a combination of the two can effectively attenuate the crosstalk.

Figure 1 compares diagonal parts of the exact Hessian (Figure 1(a)) obtained using equation 5 and the phase-encoded Hessians (Figure 1(b) for the receiver-side randomly phase-encoded Hessian and Figure 1(c) for the simultaneously phase-encoded Hessian with a mixed encoding strategy) for a simple model with a constant velocity of 2000 m/s. The acquisition geometry consists of 201 shots from -1000 m to 1000 m with a 10 m sampling and 201 receivers also spanning from -1000 m to 1000 m with a 10 m sampling. Figure 2 compares the off-diagonal elements (a row of the truncted Hessian matrix) for image point at $x = 0$ m, $z = 800$ m. The size of the filter is 21×21 in x and z directions. The comparisons show that besides lower computational cost, the phase-encoded Hessians are good approximations to the exact truncated Hessian.

REGULARIZATION WITH SPARSENESS CONSTRAINTS

Inverting the linear system defined by equation 4 is difficult, because it is underdetermined due to the incomplete subsurface illumination caused by the limited surface acquisition and complex overburden. Another difficulty arises when our Born modeling operator $\mathbf{L}$ is not sufficient to model all the complexities in the observed data $\mathbf{d}_{\text{obs}}$. For example, the commonly used one-way wave-equation propagator is based on acoustic assumption and cannot handle waves beyond 90 degrees; its amplitude is also not accurate for wide angles propagations (Zhang et al., 2005). The operator mismatch can make the inversion unstable. Of course, adding more data and using more accurate modeling operators can always help, but a more cost effective way would be introducing regularization operators that impose the *a priori* information to stabilize the inversion and make it converge to a geologically reasonable solution. A widely used regularization is the ℓ_2-norm damping, which minimizes the energy of the model parameters by introducing a secondary objective function, and the overal

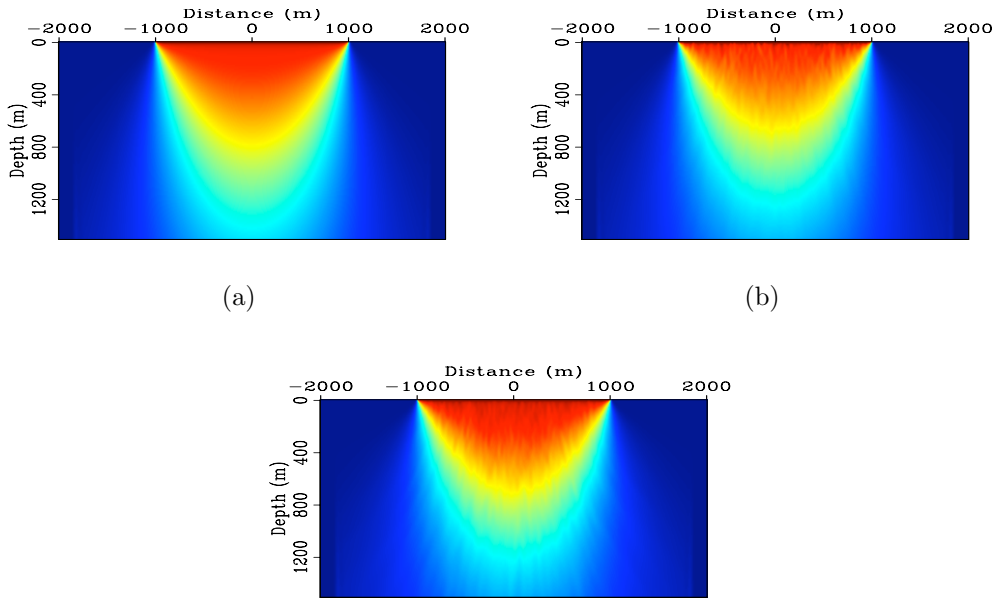

Figure 1: The diagonal part of the Hessian for a constant-velocity model. (a) The exact Hessian; (b) the receiver-side randomly phase-encoded Hessian and (c) the simultaneously phase-encoded Hessian with a mixed phase encoding which combines both random and plane-wave encoding functions. [**CR**]

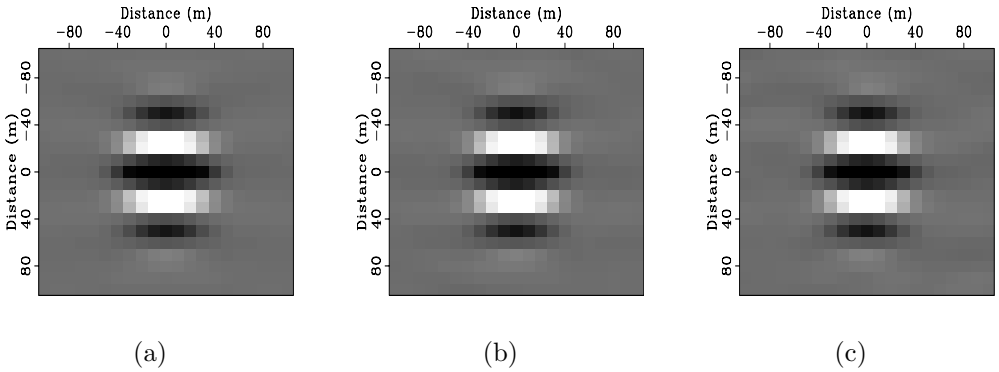

Figure 2: The off-diagonal elements of the Hessian for a image point (a row of the Hessian). (a) The exact Hessian; (b) the receiver-side randomly phase-encoded Hessian and (c) the simultaneously phase-encoded Hessian with a mixed phase encoding which combines both random and plane-wave encoding functions. [**CR**]

objective function to minimize becomes

$$J(\mathbf{m}) = ||\mathbf{Hm} - \mathbf{m}_{\text{mig}}||_2^2 + \epsilon||\mathbf{m}||_2^2, \tag{7}$$

where ϵ is a trade-off parameter that controls the strength of regularization. The ℓ_2-norm damping assumes the statistic of the reflectivity has a Gaussian distribution, which often leads to a relatively smooth solution. If we assume that the reflectivity is made up of spikes (Oldenburg et al., 1981), then the short-tailed Gaussian distribution assumption becomes unappropriate. To obtain a spiky or sparse solution, a long-tailed distribution such as exponential (the ℓ_1 norm) or Cauchy (the Cauchy norm) distribution should be used (Sacchi and Ulrych, 1995). The objective function with a regularization in the Cauchy norm reads

$$J(\mathbf{m}) = ||\mathbf{Hm} - \mathbf{m}_{\text{mig}}||_2^2 + \epsilon S(\mathbf{m}), \tag{8}$$

where $S(\mathbf{m})$ is a non-quadratic regularization function defined as follows:

$$S(\mathbf{m}) = \sum_{\mathbf{x}} \log(1 + m^2(\mathbf{x})/\sigma^2), \tag{9}$$

in which σ^2 is a scalar parameter of the Cauchy distribution that controls the sparsity of the model. The objective function 8 can be minimized under ℓ_2 norm with the iterative reweighted least-squares (IRLS) technique (Darche, 1989; Nichols, 1994; Scales and Smith, 1994; Guitton, 2000), which equivalently minimizes the following non-linear objective function:

$$J(\mathbf{m}) = ||\mathbf{Hm} - \mathbf{m}_{\text{mig}}||_2^2 + \epsilon||\mathbf{Qm}||_2^2, \tag{10}$$

where $\mathbf{Q}$ is a model dependent diagonal operator defined as follows:

$$\mathbf{Q} = \mathbf{diag}\left(\frac{1}{\sqrt{1 + m^2(\mathbf{x})/\sigma^2}}\right). \tag{11}$$

The detailed implementation of IRLS can be found in Darche (1989); Nichols (1994); Scales and Smith (1994); Guitton (2000).

NUMERICAL EXAMPLES

I test both regularized target-oriented inversion schemes (equation 7 and 8) on the Marmousi model. Two data sets are synthesized: the first one is generated using one-way wave-equation Born modeling, while the second one is generated using two-way acoustic wave-equation finite-difference modeling. Figure 3(a) shows the stratigraphic velocity model used for the two-way wave-equation modeling. Figure 3(b) and Figure 3(c) show the corresponding background velocity model (the low frequency component of Figure 3(a)) and the reflectivity model (the high frequency component of Figure 3(a)) for the one-way wave-equation Born modeling. For both data sets, I model

251 shots ranging from 4000 m to 9000 m with a 20 m sampling. The receiver spread is fixed for all shots and spans from 4000 m to 9000 m with a 10 m sampling. Figure 4 compares the modeled shot gathers located at 6500 m. Note the amplitude differences between both data. Also note that some complexities present in two-way finite-difference modeled data are not modeled using the one-way Born modeling.

The target zone selected for inversion tests is outlined with a small box in Figure 3(a), a close-up look is also shown in Figure 5(a). The target zone is where the reservoir locates. The target-oriented Hessian is computed using the receiver-side random-phase encoding (Tang, 2008b,a). The smooth background velocity model (Figure 3(b)) and the Fourier finite-difference (FFD) one-way extrapolator (Ristow and Rühl, 1994) are used for migrating both one-way and two-way data and also for the Hessian computation. Figure 5(b) illustrates the diagonal elements of the phase-encoded Hessian for the target area (the amplitude is normalized). Note the uneven illumination due to the limited acquisition geometry and complex velocity model. Figure 6 shows the truncated local Hessian filters for three different image points (three rows of the truncted Hessian). The size of the filter is 31×31 in x and z directions, which seems to be big enough to capture most of the energy in the Hessian matrix.

Figure 7 shows the inversion results on the one-way wave-equation Born-modeled data. This example represents the ideal case for one-way wave-equation inversion, since our modeling operator can "explain" all the physics present in the "observed" data (Figure 4(a)). As expected, migration produces a blurred image (Figure 7(b)); the regularized inversion schemes optimally deblur the migrated image, and the reflectivity is better recovered (Figure 7(c) and Figure 7(d)). Note that both inversion schemes enhance the spatial resolution. Also note that regularization with the sparseness constraint produces slightly higher resolution than regularization with the standard ℓ_2-norm damping and Figure 7(d) is closer to the true reflectivity shown in Figure 8(a). This suggests that the sparseness constraint better predicts the model covariance, so that it more effectively reduces the null space and provides more accurate inversion result.

More interesting and also more instructive examples are shown in Figure 8, where both regularized inversion schemes are applied to the data synthesized using the two-way wave-equation finite-difference modeling (Figure 4(b)). In this case, the one-way wave-equation migrated image (Figure 8(b)) is much noisier than the corresponding result using the one-way Born data (Figure 7(b)); the amplitudes are also more distorted. This phenomenon is due to the operator mismatch, where the internal multiples and wide angle propagations cannot be modeled by the one-way Born modeling operator. Consequently, they contribute to the artifacts shown in Figure 8(b). The operator mismatch also influences the inversion results, as shown in Figure 8(c) and Figure 8(d). The inverted images are noisier and have more artifacts compared to the results obtained on the one-way Born data. But noticeable improvement on resolution over migrated image (Figure 8(b)) can still be identified. Note that inversion regularized with the sparseness constraint seems to provide a less noisy image

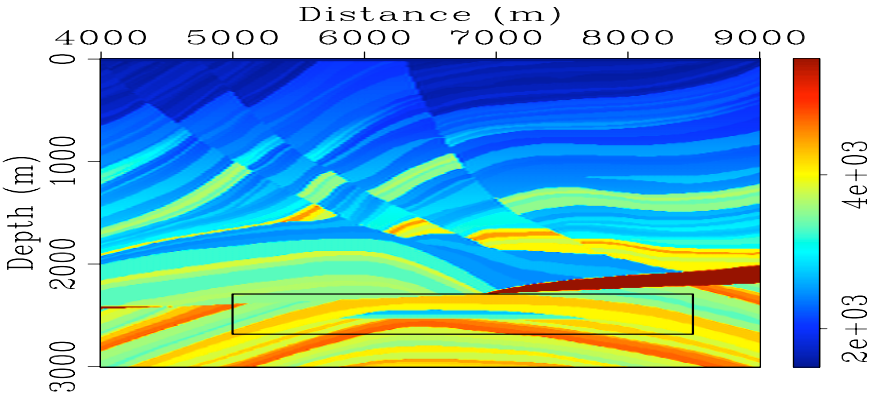

(a)

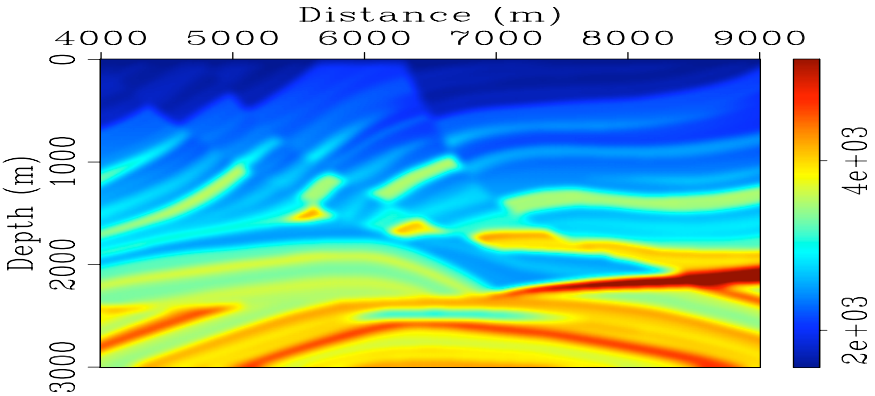

(b)

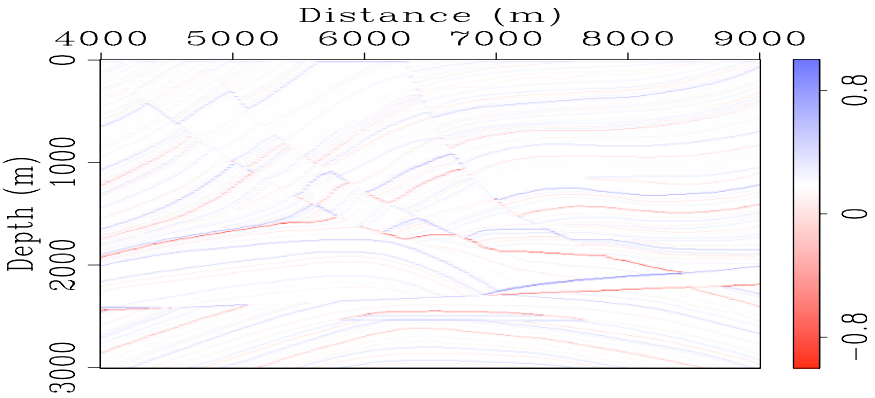

(c)

Figure 3: The Marmousi model. Panel (a) is the stratigraphic velocity model used for two-way wave-equation finite-difference modeling. Panels (b) and (c) are the background velocity model and reflectivity model used for one-way wave-equation Born modeling. [**ER**]

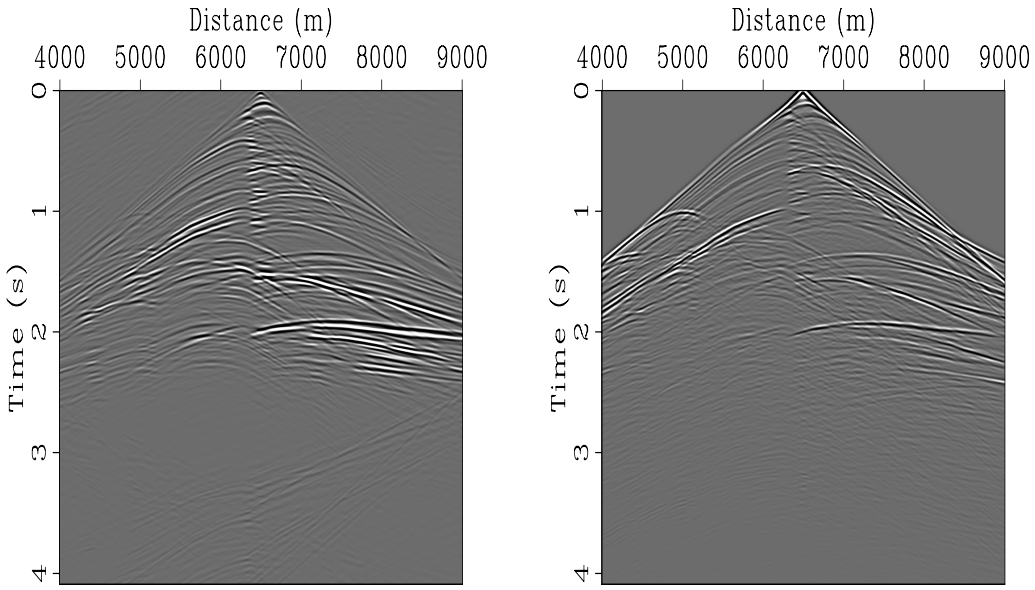

(a) (b)

Figure 4: Comparison between shots synthesized using (a) one-way wave-equation Born modeling and (b) two-way wave-equation finite-difference modeling. [**CR**]

with slightly higher spatial resolution than the inverted image regularized with the ℓ_2-norm damping. This example suggests that when we have operator mismatch issues for inverse problems, it is important to add regularization operators that more accurately predict the model covariance. In this particular example, although promoting sparsity may not be the best regularization, it does better predicts the model covariance than the ℓ_2-norm damping, hence it produces a better result even when our operator is not able to fully explain the observed data.

DISCUSSION

This paper presents a sparseness constrained LSI scheme that promotes sparsity of the reflectivity. This is a reasonable assumption if the reflectivity is indeed spiky; however, if the reflectivity changes smoothly, the sparseness constraint may lead to a biased solution. The parameters σ and ϵ that control the strength of sparsity and the amount of regularization should also be chosen with extreme care. Because by promoting sparsity, we run the risk of penalizing true reflections that have very weak energy, over-regularization may lead to too-sparse solutions, forfeiting the ability to image weak reflections.

Recent study in curvelet (Kumar and Herrmann, 2008) and seislet (Fomel, 2006) transforms show that seismic images tend to have a sparse representation in these new

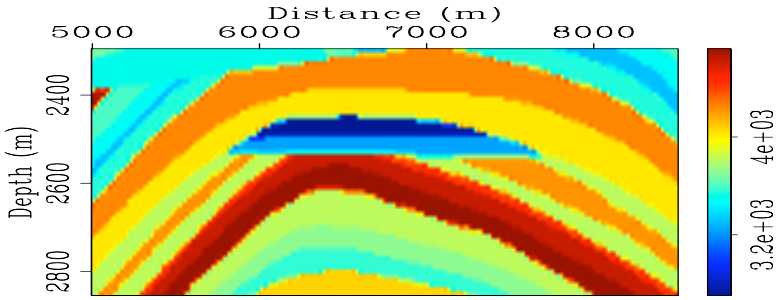

(a)

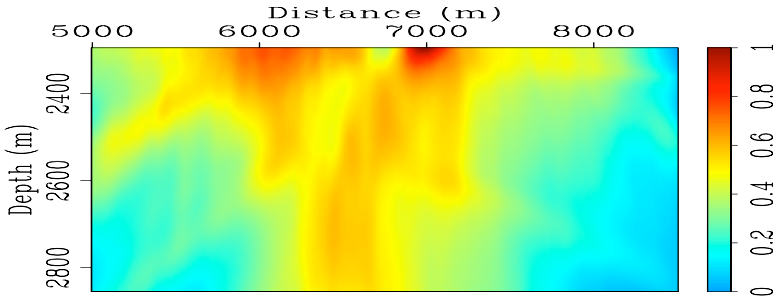

(b)

Figure 5: (a) The stratigraphic velocity model for the target zone. (b) The diagonal of the Hessian for the target zone. [**CR**]

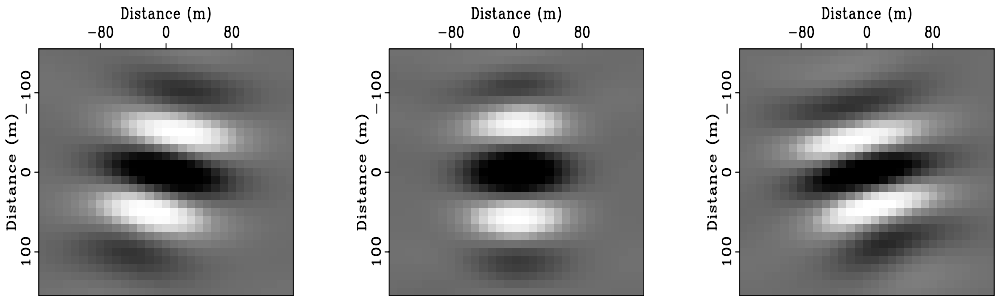

(a) (b) (c)

Figure 6: The local Hessian filters at (a) $x = 5250$ m, $z = 2800$ m, (b) $x = 6500$ m, $z = 2600$ m and (c) $x = 8400$ m, $z = 2400$ m. [**CR**]

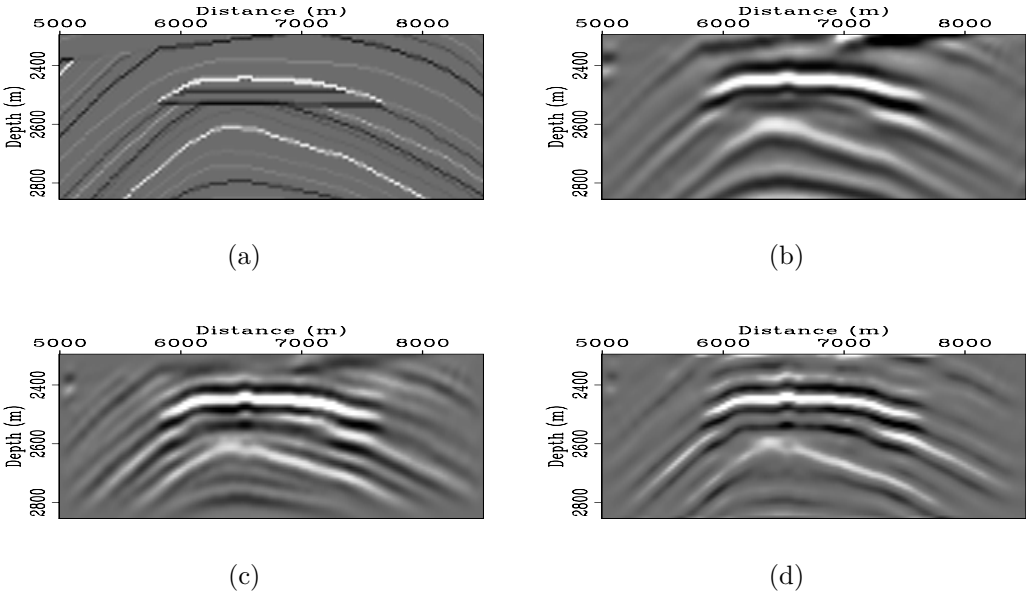

Figure 7: Target-orineted inversion of the one-way wave-equation Born-modeled data. (a) The true reflectivity, (b) migration, (c) inversion regularized with ℓ_2 norm damping (equation 7) and (d) inversion regularized with the sparseness constraint (equation 8). [**CR**]

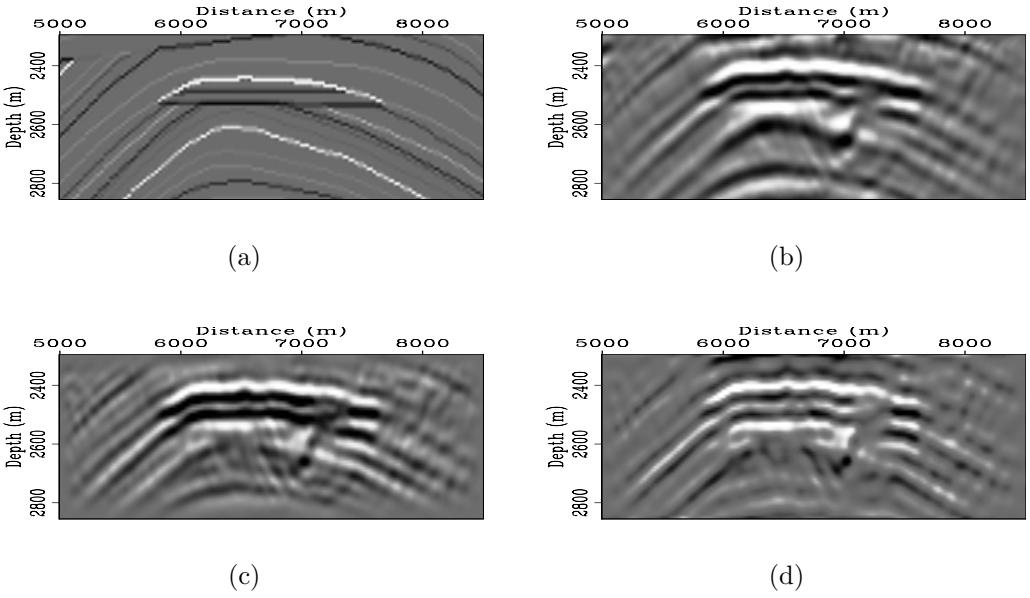

Figure 8: Target-orineted inversion of the two-way wave-equation finite-difference modeled data. (a) The true reflectivity, (b) migration, (c) inversion regularized with ℓ_2 norm damping (equation 7) and (d) inversion regularized with the sparseness constraint (equation 8). [**CR**]

domains, where a few number of coefficients are sufficient to describe images with complex structures. This feature makes these new domains good candidates for adding sparseness constraints. Therefore, promoting sparsity in either curvelet or seislet domain may potentially avoid the issues discussed before and lead to geologically more reasonable solutions. This remains a research area for further investigation.

CONCLUSIONS

I have presented a regularized least-squares inversion scheme to image the reflectivity. This inversion scheme allows us to perform inversion in a target-oriented fashion, and the total cost is about two migrations (one for computing the migrated image, the other for computing the phase-encoded Hessian). Examples on the Marmousi model show that regularization that promotes sparsity in the image domain help to reduce the null space and to mitigate the effects of operator mismatch. Inversion with the sparseness constraint can lead to a better solution with higher resolution than that regularized with the standard ℓ_2-norm damping.

REFERENCES

Amundsen, L., 1991, Comparison of the least-squares criterion and the Cauchy criterion in frequency-wavenumber inversion: Geophysics, **56**, 2027–2035.

Claerbout, J. F., 1985, Imaging the earth's interior: Blackwell Scientific Publication.

Clapp, M. L., 2005, Imaging Under Salt: Illumination Compensation by Regularized Inversion: PhD thesis, Stanford University.

Darche, G., 1989, Iterative L1 deconvolution: **SEP-61**, 281–301.

Fomel, S., 2006, Towards the seislet transform: SEG Technical Program Expanded Abstracts, **25**, 2847–2851.

Guitton, A., 2000, Huber solver versus IRLS algorithm for quasi L1 inversion: **SEP-103**, 205–266.

Kuhl, H. and M. D. Sacchi, 2003, Least-squares wave-equation migration for AVP/AVA inversion: Geophysics, **68**, 262–273.

Kumar, V. and F. J. Herrmann, 2008, Deconvolution with curvelet-domain sparsity: SEG Technical Program Expanded Abstracts, **27**, 1996–2000.

Lailly, P., 1983, The seismic inverse problem as a sequence of before stack migration: Proc. Conf. on Inverse Scattering, Theory and Applications, Expanded Abstracts, Philadelphia, SIAM.

Nemeth, T., C. Wu, and G. Schuster, 1999, Least-squares migration of incomplete reflection data: Geophysics, **64**, 208–221.

Nichols, D., 1994, Velocity-stack inversion using Lp norms: **SEP-82**, 1–16.

Oldenburg, D. W., S. Levy, and K. P. Whittall, 1981, Wavelet estimation and deconvolution: Geophysics, **46**, 1528–1542.

Plessix, R.-E. and W. A. Mulder, 2004, Frequency-domain finite-difference amplitude-preserving migration: Geophys. J. Int., **157**, 975–987.

Ristow, D. and T. Rühl, 1994, Fourier finite-difference migration: Geophysics, **59**, 1882–1893.

Sacchi, M. D. and T. J. Ulrych, 1995, High-resolution velocity gathers and offset space reconstruction: Geophysics, **60**, 1169–1177.

Scales, J. A. and M. L. Smith, 1994, Introductory geophysical inverse theory: Samizdat Press.

Stoffa, P. L., J. T. Fokkema, R. M. de Luna Freire, and W. P. Kessinger, 1990, Split-step fourier migration: Geophysics, **55**, 410–421.

Tang, Y., 2006, Least-squares migration of incomplete data sets with regularization in the subsurface-offset domain: **SEP-125**, 159–175.

———, 2008a, Modeling, migration and inversion in the generalized source and receiver domain: **SEP-136**, 97–112.

———, 2008b, Wave-equation Hessian by phase encoding: **SEP-134**, 1–24.

Tang, Y. and B. Biondi, 2009, Least-squares migration/inversion of blended data: **SEP-138**.

Ulrych, T. J., M. D. Sacchi, and A. Woodbury, 2001, A Bayes tour of inversion: A tutorial: Geophysics, **66**, 55–69.

Valenciano, A., 2008, Imaging by Wave-equation Inversion: PhD thesis, Stanford University.

Wang, J. and M. D. Sacchi, 2007, High-resolution wave-equation amplitude-variation-with-ray-parameter (AVP) imaging with sparseness constraints: Geophysics, **72**, S11–S18.

Yu, J., J. Hu, G. T. Schuster, and R. Estill, 2006, Prestack migration deconvolution: Geophysics, **71**, no.2, S53–S62.

Zhang, Y., G. Zhang, and N. Bleistein, 2005, Theory of true-amplitude one-way wave equations and true-amplitude common-shot migration: Geophysics, **70**, E1–E10.